ISSN 1027-4510, Journal of Surface Investigation. X-ray, Synchrotron and Neutron Techniques, 2014, Vol. 8, No. 3, pp. 444–455. © Pleiades Publishing, Ltd., 2014.
Original Russian Text © L.I. Goray, M.N. Lubov, 2014, published in Poverkhnost'. Rentgenovskie, Sinkhrotronnye i Neitronnye Issledovaniya, 2014, No. 5, pp. 39–51.

Nonlinear Continual Growth Model of Nonuniformly Scaled Reliefs as Applied to the Rigorous Analysis of the X-ray Scattering Intensity of Multilayer Mirrors and Gratings

L. I. Goray[a, b] and M. N. Lubov[a, c]

[a] *St. Petersburg Academic University–Nanotechnology Research and Education Centre, Russian Academy of Sciences, St. Petersburg, Russia*

[b] *Institute for Analytical Instrumentation, Russian Academy of Sciences, St. Petersburg, Russia*

[c] *Ioffe Physical Technical Institute, Russian Academy of Sciences, St. Petersburg, Russia*

Received May 30, 2013

Abstract—It is revealed that certain terms entering into the nonlinear continual equation describing thin-film growth enable its application to the simulation of the surfaces of multilayer mirrors and gratings with a large height and/or jumps of boundary-profile gradients. The proposed model characterizes both variations in the power spectral-density function of the surface of Al/Zr multilayer mirrors and the smoothing and shift of the boundaries of Mo/Si and Al/Zr gratings grown on Si substrates with triangular groove profiles by means of magnetron and ion-beam deposition. Rigorous calculations indicate that the intensities of diffuse X-ray scattering by Au mirrors, which have similar boundary profiles with Gaussian and exponential autocorrelation functions, differ substantially from each other. Computer simulation of the growth of Mo/Si and Al/Zr multilayer gratings is performed. On the basis of the calculated boundary profiles, the absolute diffraction efficiencies of the Mo/Si and Al/Zr gratings are found via the integral equation method in the extreme UV region. It is demonstrated that the proposed comprehensive approach to calculations of the boundary profiles and the intensities of short-wavelength scattering from multilayer mirrors and gratings makes it possible to carry out studies comparable in accuracy to measurements based on synchrotron radiation.

DOI: 10.1134/S1027451014030057

INTRODUCTION

Progress in the manufacture of X-ray multilayer diffraction gratings and mirrors with preselected boundary shapes and assigned subatomic roughnesses is related first of all to the holographic and lithographic methods used in the production thereof, advances in material chemistry, the advancement of vacuum techniques and technology for preparing and treating Si plates, and achievements in nanometrology. Further investigations are urgent because there is a necessity to create up-to-date high-resolution and high-efficiency components for optical and electronic devices (including those for 6.X-nm lithography) and X-ray free-electron lasers and develop resonant inelastic X-ray scattering, soft X-ray and extreme UV (EUV) astrophysics, X-ray microscopy, and other fields of application. The comparison of scattering intensities measured with the help of synchrotron-radiation (SR) sources and X-ray free-electron lasers with data calculated via rigorous methods becomes more and more important for short-wavelength optics.

It should be emphasized that microscopy methods, such as transmission electron microscopy (TEM), atomic-force microscopy (AFM), and near-field scanning optical microscopy, are finding wide application in qualitative research into the evolution of thin-film boundary profiles. The first approach is expensive and destructive, and the other two techniques make it impossible to determine the boundary profiles of the internal layers of prepared samples. Moreover, only the local characteristics of a formed structure can be studied with the use of microscopy methods.

The most universal approach to examination of the morphology and composition of layers is the reflectometry (scatterometry) method, including its short-wavelength variant whereby the nanorelief characteristics of practically all thin-film materials can accurately be determined in an integrated way [1]. When solving the imperfectly and ambiguously defined inverse problems of reflectometry [2], it is especially important to have a universal and rigorous method for solving a direct problem and information on the recovered relief and/or refractive indices of the materials, which are employed as an initial approximation. Despite the substantial progress in the development of accurate numerical methods for examining wave diffraction by arbitrary boundary asperities achieved in the last few years [3], the X-ray and neutron scattering intensities have only recently been analyzed by means of asymptotic and approximate approaches: the Kirchhoff scalar integral method, the Born approximation, the distorted-wave Born approx-

imation, parabolic equation and Rayleigh methods, and certain other techniques [1, 4]. As a rule, the intensities of X-ray scattering at crystalline structures are theoretically predicted using formalism based on the Takagi–Taupin equation, which was extended to deformed crystals and strained layers [1]. However, such an approach does not depend explicitly on the boundary-profile parameters and their horizontal and vertical correlation and provides no way of determining the absolute values of the intensities of scattering at amorphous and other noncrystalline layers. The modified boundary integral approach (MBIA) [5–7], which is used to analyze how the boundary profiles of gratings and mirrors with complex, rough interfaces affect the X-ray scattering intensity, is a new technique based on the optical theory of continuous media, i.e., solution to the Maxwell equations with strict boundary and radiation conditions. With the help of the MBIA, it was demonstrated that, at the boundaries of periodic and random relief components, the X-ray scattering intensities can differ appreciably (severalfold) from the values corresponding to various approximate models. This technique turned out to be equally applicable to different nanoroughnesses characterized by the arbitrary (not necessarily periodic or Gaussian) statistics of distribution and shape proposed in [4]. Our research is focused on the significant discrepancies between the MBIA and the known boundary integral approaches and the peculiarities arising from its applications to analysis of the intensity of short-wavelength scattering at mirrors and gratings. A comprehensive description of the MBIA can be found in the aforementioned references.

The intensities of X-ray scattering ay multilayer mirrors and gratings are commonly calculated using the layer-boundary profiles obtained upon transition from the initial to final profile scales within the scope of various scaling models [8–10]. In such calculations, there are often no accurate data on the initial or final boundary profile. Hence, the fitting of internal boundary profiles is markedly sophisticated [11]. Such an approach makes it impossible to allow for source noise having a considerable influence on the growth process, the shift of large-scale grating profiles due to profile smoothing or changes in the angle of material deposition onto the grating, and variations in the surface relaxation parameters during the growth period.

To describe the formation of relief surfaces, the combined use of theoretical techniques and computer simulation methods is the most efficient approach [12–14] ensuring detailed investigation of the growth process and the acquisition of accurate quantitative data on the boundary profiles. The thin-film boundary profile evolution is generally described using three basic approaches: a discrete (kinetic Monte Carlo) method, a dynamic technique involving classical and quantum molecular dynamics methods, and a continual (continuous) approach [15–17]. In this study, the thin-film profile evolution is simulated via the continual approach, because, in contrast to discrete and dynamic methods, it enables us to calculate the relief evolution over long time intervals ($\sim 10^3$ s) and on large spatial scales (~ 10 μm). In addition, the continuous model provides an opportunity to directly examine how the growth process depends on the source noise and various nonlinear and geometric effects. Thus, for complex profiled surfaces like X-ray multilayer diffraction gratings with random roughness, we assume that the application of a complex theoretical approach is quite advisable. This is because such a technique can almost completely replace an experiment and makes it possible to calculate both the layer-boundary profile evolution and the optical response of the boundaries by means of short-wavelength reflectometry.

The goal of this study is the theoretical investigation and computer simulation of boundary growth and the intensity of short-wavelength scattering at multilayer mirrors and gratings on the basis of the method proposed by the authors. In this study, for the first time, the diffraction efficiency $\eta(\#)$ corresponding to the #th order of multilayer mirrors and gratings is calculated with the use of boundary profiles obtained by simulating the growth of layer boundaries. Below, the continual equation, which describes the evolution of the profiles of small-scale (rough mirror) and large-scale (grating) reliefs, is proposed and investigated.

MODEL OF THIN-FILM GROWTH ON PROFILED SURFACES

Mechanisms of the Growth and Relaxation (Smoothing) of a Thin-Film Profile

When growing a thin film, the evolution of its boundary profile is controlled by two processes. The first is deposition leading to an increase in profile height reckoned from the initial level h_0, and the second is relaxation that smoothes irregularities on the film surface. Surface relaxation is caused by the fact that a growing system (thin film) tends to the thermodynamic state characterized by identical chemical potentials $\mu(\mathbf{r}, t)$ at all points $\mathbf{r}$ of the surface. The main relaxation mechanisms are surface diffusion, a simultaneous evaporation and condensation process, and bulk diffusion [12, 18]. For the given material system, the basic mechanism of surface relaxation is determined by the growth conditions (substrate temperature, deposition rate, etc.) because the diffusion and evaporation rates depend on the temperature and concentration of adatoms on the substrate. The migration barriers of atomic diffusion in the film bulk are higher than those inherent to its surface. Therefore, the influence of bulk diffusion on variations in the film profile is much weaker than that of surface diffusion. Hence, for simplicity, bulk diffusion is excluded from further consideration.

As is known, the chemical potentials of atoms on planar and curved surfaces (respectively, $\mu_p(\mathbf{r}, t)$ and

$\mu_c(\mathbf{r}, t)$) are connected by the Gibbs–Thomson relationship [19]:

$$\mu_c(\mathbf{r}, t) = \mu_p(\mathbf{r}, t) - 2\gamma K(\mathbf{r}) V_m, \quad (1)$$

where γ is the specific surface energy, $K(\mathbf{r})$ is the local curvature of the surface, and V_m is the molar volume.

It is assumed that a 2D surface is isotropic, i.e., quantity h can be defined by coordinate x and time t. In the simplest case where relaxation occurs by the evaporation–condensation mechanism, the rate of height change, $\partial h(x,t)/\partial t$, can be written as [18]

$$\partial h(x, t)/\partial t = -\nu_2 \sqrt{1 + [\nabla h(x, t)^2]} K(x), \quad (2)$$

When relaxation proceeds by the diffusion mechanism, we obtain

$$\partial h(x, t)/\partial t = \nu_4 \sqrt{1 + [\nabla h(x, t)^2]} [\partial^2 K(x)/\partial x^2]. \quad (3)$$

In Eqs. (1) and (2), parameter ν_2 specifies the evaporation–condensation rate and ν_4 is the diffusion rate.

Note that Eqs. (1) and (2) can be simplified if $h(x, t)$ depends weakly on x (the small-angle approximation), i.e.,

$$\nabla h(x,t) \ll 1, \quad (4)$$

It is known that quantity $K(x)$ is defined as [20]

$$K(x) = -\frac{\nabla^2 h(x, t)}{(1 + \nabla h(x, t))^{3/2}}, \quad (5a)$$

Therefore, applying the small-angle approximation to (5a), we obtain

$$K(x) = -\nabla^2 h(x, t). \quad (5b)$$

Let us write the equation for the film-profile evolution observed at small slope angles of the profile, i.e., in the small-angle approximation (4), under the assumption that variations in the film profile are initiated by three processes: deposition, simultaneously occurring evaporation and condensation, and diffusion. With allowance for film material deposition on the substrate, the substitution of (4) into (2) and (5b) into (3) provides changes in the film height with time t:

$$\partial h(x, t)/\partial t = g(x, t) + \nu_2 \nabla^2 h(x, t) - \nu_4 \nabla^4 h(x, t), \quad (6)$$

where $g(x, t)$ is the random function of an atomic flux incident on the film surface. The behavior of function $g(x, t)$ depends on the source type. However, in the majority of cases, it can be assumed that the atomic flux fluctuates near the average value $\langle g(x,t) \rangle = I_0$ and flux fluctuations I (noise) are uncorrelated:

$$\langle \delta g(x, t) \delta g(x', t') \rangle = I \delta(x - x') \delta(t - t'), \quad (7)$$

where δ is the Dirac delta function.

When a film grows along the normal to its local surface, the film profile evolution cannot be correctly described using (6). Kardar, Parisi, and Zhang were the first scientists to propose a nonlinear equation for correctly estimating the lateral growth contribution to variations in a film profile:

$$\partial h(x, t)/\partial t = g(x, t) + \nu \nabla^2 h(x, t) + \Lambda [\nabla h(x, t)]^2, \quad (8)$$

where Λ is the relaxation parameter. In Eq. (8), the second term of the right-hand side characterizes film profile smoothing under the action of surface-tension forces. In this case, as in (6), the small-angle approximation is applied to (8). It should be noted that there are several nonlinear equations analogous to (8), e.g., the Kuramoto–Sivashinsky equation [12] describing how the spatially ordered relief ("pattern") is formed on the film surface during its growth.

The general form of the equation characterizing time variations in the profile depends on the physical processes observed on the film surface and in its volume. In particular, it is necessary to employ other expressions for diffusion terms if a substrate surface contains spikes of different height, between which occurs the exchange of atoms. In the general case, the equation for film evolution takes the form

$$\partial h(\mathbf{r}, t)/\partial t = g(\mathbf{r}, t) + f(\nabla h(\mathbf{r}, t), \nabla^2 h(\mathbf{r}, t), \ldots). \quad (9)$$

Here, function f describes the film-surface relaxation and is the sum of linear and nonlinear terms (respectively, $\nabla^n h(\mathbf{r},t)$ and $\nabla^l([\nabla^n h(\mathbf{r},t)]^k)$, where l, k, and $n \in N$). The peculiar form of function f is determined by the type of physical processes occurring in the system.

Simulation of the Growth of X-Ray Multilayer Mirrors and Gratings

In the manufacture of multilayer mirrors and gratings employed in X-ray optics, the shape and roughness of the lower and upper boundaries and internal interfaces between layers must be strictly controlled. The short-wavelength scattering intensity of the aforementioned multilayer structures is affected by both small-scale relief arising from the influence of source noise and nonideality of the substrate, and also the large-scale relief of the grating grooves. Hence, when the evolution of boundary profiles inherent to multilayer mirrors and gratings is studied theoretically, it is necessary to carry out rigorous numerical simulation of the growth process, which allows for the features listed above.

The working-face angle φ of typical high-frequency gratings with triangular groove profiles, which are widespread in short-wavelength optics, is several degrees. In this case, the opposite base angle β of the triangle is several tens of degrees. At these angles between the profile and the grating plane, the small-angle approximation (4) becomes incorrect. Hence, the local curvature of the surface must be described by expression (5a). In connection with this, with allowance for two mechanisms of surface relaxation speci-

fied by (2) and (3), the equation for surface profile evolution can be represented as

$$\partial h(x,t)/\partial t = g(x,t) - \nu_2\sqrt{1+[\nabla h(x,t)]^2}K(x) + \nu_4\sqrt{1+[\nabla h(x,t)]^2}\left[\partial^2 K(x)/\partial x^2\right]. \quad (10)$$

An analogous equation must be employed to simulate the growth of multilayer mirrors that are often characterized by quantity $\nabla h(x,t) \sim 1$, e.g., at large rms deviations σ and small correlation lengths ξ of the surface roughness.

When the growth of multilayer gratings is simulated, there is a need to correctly allow for both the local curvature and the angle of incidence of the deposited atoms. This is associated with the fact that the grating groove geometry can give rise to inhomogeneous material deposition on the substrate as a result of shadowing effects [21]. To decrease the influence of deposition inhomogeneity on the growth process, the angle between the incident atomic beam and the growth face of the grating groove must be close to 90°. However, in real growth setups, it is extremely difficult to achieve optimal deposition angles. Hence, the shadowing effects are reduced by means of oblique deposition on the nonworking groove face tilted to the substrate plane at a significantly larger angle.

Let us calculate the fluxes deposited onto a triangular profile under the assumption that an atomic flux impinges on the substrate plane at angle α and $\beta > \varphi$. To eliminate working-face shadowing, the generally accepted condition $\alpha > \varphi$ must be fulfilled. In this case, without allowance for noise, the number of atoms deposited on the working face is determined from the formula

$$g = I_0 \sin(\alpha - \varphi(x, t)), \quad (11a)$$

where $\varphi(x, t) = \text{arctg}(\nabla h)$ is the angle of the slope of the working face at the point with coordinate x at instant t.

For an atomic flux incident on the nonworking face, we obtain

$$g = I_0 \sin(\alpha + \beta(x, t)), \quad (11b)$$

where $\beta(x, t) = \text{arctg}(|\nabla h|)$ is the angle of the slope of the nonworking face at point x at instant t.

An important characteristic, which has substantial influence on the roughness of multilayer mirrors and gratings, is the difference between the values of relaxation parameters corresponding to layer materials. For example, the surface diffusion of material *1* over a layer of material *2* can be much lower than the diffusion of material *2* over the surface of the layer fabricated from material *1*. In this case, the relaxation parameters can vary during growth. In particular, magnetron deposition can heat the near-surface layer of the growing mirror, thereby leading to changes in the diffusion coefficients and, consequently, the relaxation parameters. Moreover, the large-scale roughness can shadow adjacent surface regions, where the film growth process is altered. With the use of this specific sputtering technique and setup, other physicochemical processes can appear and should be taken into account.

Analysis of Statistics of the Film Boundary Profile

During the final stage of investigations of the growth process, it is necessary to describe the topology of the grown film. For this purpose, numerical data on boundary profiles, which are acquired by simulating film growth, are employed to find quantities capable of statistically characterizing the surface relief. By calculating the dependences between these quantities and the film thickness or the deposition time, it is possible to infer how its growth occurs.

It is assumed that variations in the film (e.g., multilayer mirror) roughness are characterized by the power spectral-density function (PSDF) $S(f, t)$ with a spatial frequency of f_x [22]:

$$S(f_x, t) = \lim_{L\to\infty}\left\langle\frac{2}{L}\left|\int_{-L/2}^{L/2} e^{2\pi i x f_x} h(x, t)dx\right|^2\right\rangle, \quad (12a)$$

where L is the spatial size of the mirror, quantity f_x varies from $1/L$ to $n/2L$, and n is the number of points used to specify the mirror profile. The rms deviations σ of the roughness are calculated with the help of $S(f, t)$:

$$\sigma^2(t) = 2\int_{1/L}^{n/2L} S(f_x, t)(df_x). \quad (12b)$$

In this approach, the roughness correlation length ξ is chosen to be the reciprocal of the frequency corresponding to the inflection point of function $S(f, t)$. The length ξ can be easily determined by fitting analytical function $S_{\text{An}}(f_x, t)$ to the function $S(f, t)$ obtained from calculations of $h(x, t)$. For this purpose, let us take advantage of the K-correlation model [22]:

$$S_{\text{An}}(f_x, t) = \frac{A}{(1 + \xi_{\text{An}} f_x^2)^{B/2}}, \quad (12c)$$

where A and B are the fitting parameters and ξ_{An} is the correlation length of fitting.

When initial conditions are assigned, it is often accepted that the probability density function of roughness heights is described by the Gaussian function

$$f_h(x) = \frac{1}{\sigma\sqrt{2\pi}}\exp\left\{-\frac{x^2}{2\sigma^2}\right\}, \quad (13a)$$

and the autocorrelation function has an exponential form:

$$C(x) = \sigma^2 \exp\left\{\frac{x^{2D}}{\xi^{2D}}\right\}, \quad (13b)$$

where $0 < D \leq 1$ is the Hurst exponent (the scaling parameter of roughness). Function $C(x)$ is interpreted as a Gaussian autocorrelation function if $D = 1$ and is an exponential function if $D = 0.5$.

RIGOROUS THEORY OF SCATTERING AT MULTILAYER GRATINGS WITH RANDOM ROUGHNESS

Below, the necessary description of the MBIA theory is brief because its basic parts, including the peculiarities of rigorous solution to the short-wavelength diffraction problems (i.e., problems concerned with a small ratio between wavelength λ and grating period d or correlation length ξ), are thoroughly reviewed in [5–7]. The electromagnetic formulation of the grating (infinite periodic structure) diffraction problem is reduced to a set of Helmholtz equations for the z components of electric and magnetic fields in R^2. Its solution is quasi-periodic in the x direction, is defined by radiation conditions in the y direction, and satisfies strict boundary conditions at the interfaces between different materials. A multilayer grating can have a very large number of boundaries, namely, up to several thousand in its application to hard X-rays. In the case of classical diffraction where the wave vector of an incident wave is perpendicular to the z direction, the system is divided into two independent problems corresponding to two fundamental polarization states. However, for conical diffraction, the boundary values of the z components of fields and their normal and tangential derivatives are related to each other [23, 24]. The grating diffracts an incident wave into a finite number of outgoing (so-called reflected) plane waves and, presumably, several transmitted modes (orders). For an arbitrary number of layers with different boundaries, including polygonal ones, determined from measurements or growth simulation, the energies of orders and the absorption are calculated by means of the PCGrate-SX 6.5 software [25].

The influence of roughness on the scattering efficiency is accurately taken into account using the model in which a rough surface is interpreted as a grating with the large period d and containing an appropriate number of random asperities. The PCGrate® program analyzes complicated structures, which are interpreted both as multilayer gratings (from a mathematical viewpoint) and, simultaneously, as rough surfaces at $d \gg \xi$. When $\xi \sim \lambda$ and the number of orders is high, the continuous angular distribution of the energy reflected from randomly rough boundaries is described by the discrete distribution $\eta(\#)$ of the grating [6]. The MBIA study of the scattering intensity begins with determining the statistical implementations of the profile boundaries of the examined structure. Then, the intensity of each implementation is calculated. Afterward, the intensities are averaged over all implementations. The properties of the rough surface are averaged by selecting sufficiently extended samples. However, this approach has no approximations, including Monte Carlo averaging. The more general case of double-period gratings (3D surfaces) can be analyzed in a similar way or by expressing the solution to the 3D Helmholtz equation in terms of solutions to the 2D equation described below. Note that the latter is quite acceptable in certain situations [2].

As is well known, great difficulties emerge if the 2D Helmholtz equation is numerically solved via any of the rigorous methods at small λ/d ratios. Although the boundary integral approach [26] is commonly stable, reliable, and efficient, its convergence and accuracy deteriorate in the short-wavelength range because quadrature calculations are accompanied by the error accumulation in digits. When gratings are analyzed in the soft X-ray and EUV regions, an increase in the matrix size and an improvement in computational accuracy, as well as the application of convergence acceleration methods which are efficient in the long- and medium-wavelength ranges, imposes unreasonably strict requirements on the used computer time and memory.

In calculations of fine-structure boundaries with depths of $h \gg \lambda$, these requirements become more strict especially if the number of grating layers increases. In this case, in the traditional integral method, at least one collocation point falls at wavelength λ (the number N of collocation points specified within one period is a basic parameter characterizing the method accuracy [6]). At the same time, the MBIA is rapid and reliable at $N\lambda/d \ll 1$ in the soft X-ray and EUV regions. For example, only 1.E–3 points are employed in the MBIA if $N = 1000$ and $\lambda/d =$ 1.E–6. In this case, however, the effective boundary depth is $h\cos\theta$ (the angle θ of incidence on the grating is reckoned from the normal to the substrate), and the multilayer coating period Δ and λ must have the same order of magnitude, at which the efficiency reaches high values in a certain order.

This inference is valid for both echelettes operating in higher orders at any wavelength λ and gratings applicable to longer wavelengths [7].

In the MBIA, the problem described by the set of Helmholtz equations is reduced to a set of integral operator equations for boundary profiles. Our technique combines a direct method (due to use of the second Green formula) and an indirect approach based on the potentials of single and double layers [7]. A solver operates only with the boundary values of fields and their derivatives. The fields of layers can be found using their values at the boundaries and from the Green formula. Let us apply the sweep method in upward and downward directions in combination with

recursive formulas for initial fields and their normal derivatives [5]. In practice, the convergence and accuracy of calculations of the efficiency η is noticeably dependent on an appropriately chosen basis, sampling scheme, and the corresponding quadrature calculation rule. One of the commonly used collocation techniques is the method of moments using a uniform distribution of points along the abscissa axis or the surface. The integral equations of the PCGrate® program are discretized via the Nyström collocation procedure, in which the integral operators are approximated by superimposing collocation points onto quadrature nodes [26]. Unknown variables are sought as piecewise-constant polynomials. Such a direct discretization method combined with the simplest rule of integral calculations according to the method of trapezoids (rectangles) operates well at $\lambda/d \ll 1$ especially if the grating grooves are not deep [5]. In the case of boundary profiles with ribs (i.e., polygonal profiles), quadrature nodes are selected so that ribs lie in the middle between neighboring points and the profile curvature is not corrected in calculating diagonal elements of the normal derivatives of Green's functions [7]. For gratings with deep grooves, it is possible to employ another variant of quadrature formulas: collocation points are located in the nodes of the ribs, and the normal derivatives of Green's functions are added to the term taking into the curvature contribution. In this case, there is also another approach, in which collocation points are joined to the rib, e.g., in geometric progression, and the relevant integration rule is implemented [23, 26].

As is known from the theory of integral equations, it is necessary to allow for the logarithmic dependence arising in nuclei due to the coincidence of arguments, the curvature profile in the diagonal elements of the normal derivative of Green's functions, and the accelerated convergence of expansion related to the residual sum excluded during the cutoff of series. The regular correction of the aforementioned expansion terms enables the obtainment of rapidly converging high-accuracy results in the resonance regions [23–28]. In the short-wavelength range, especially in the soft X-ray and EUV regions where fields with flattened envelopes strongly oscillate and rapidly decay in the direction from the grating surface with increasing order number, serious difficulties arise in an attempt to allow for these oscillations by means of the conventional integral method. These difficulties can be surmounted using the approach proposed by the authors and differing in principle from other methods. This technique relies on the fact that, in the absence of resonance, the accelerated convergence attained by correcting separate terms of expansion can be eliminated at small values of $N\lambda/d$. On the contrary, such unjustified improvement decelerates the convergence or leads to the divergence of results [7].

An additional parameter characterizing the convergence and accuracy of results is the number M of positive and negative summands in the expansion of Green's functions and their normal derivative corresponding to upper and lower media.

In the spectral range under consideration, the real part of the refractive indices of all materials is close to unity. Hence, for vacuum or any coating material, the same number M can be employed in the expansion of nuclei. Since rapidly oscillating integrands were established to be poorly integrated [29], a higher accuracy is achieved if the number of like-sign terms of nucleus expansion is less than the matrix size. Otherwise, the results begin to diverge. On the other hand, an insufficient number of terms of series expansion makes it impossible to precisely determine how the mutual influence of regions of an infinite grating contributes to the decision. The performed investigations indicate that, according to the energy balance and efficiency, $M = N/2$ ensures higher accuracy in the X-ray spectral region. This effect was called the "golden" rule [11, 30]. Note that the time spent calculating $\sim 2MN^2$ and $M = 2N/3$ was presented in [28].

SIMULATION OF THE BOUNDARY GROWTH OF MULTILAYER MIRRORS AND GRATINGS AND THE INTENSITY OF SHORT-WAVELENGTH SCATTERING

Simulation of the Diffuse Scattering Intensity of Au Mirrors

Let us demonstrate that multilayer mirrors and gratings must be developed with allowance for the statistics of film-surface roughness. For this purpose, it is necessary to calculate the intensity of the diffuse scattering at Au mirrors with two types of model roughness, which resembles real conditions and has a Gaussian amplitude distribution and a Gaussian or exponential autocorrelation function. The dependences between the calculated diffuse reflection coefficients and the grazing angle of scattering are presented in Fig. 1. The curves were determined near the critical grazing angles of incident radiation, namely, $\tau_{inc} = 90° - \theta_{inc} = 1°$ and $\tau_{inc} = 3°$, at the wavelength $\lambda = 1.54$ nm under the TE polarization condition (TM polarization exhibits analogous data). The intensities of the small-angle X-ray scattering of generated Au surfaces were calculated at $\sigma = 1$ nm, $\xi =$ 15 nm, and $D = 1$ and 0.5. The averaged intensities were calculated via the Monte Carlo method using up to 200 statistical samples of profiles with 1000 points each for an interval of 1 μm. To allow for the complicated structure of a rough surface and achieve the convergence of results, N was chosen to be 2000 in the PCGrate-SX 6.5 program.

From comparison of curves in Fig. 1, it is obvious that the diffuse reflection coefficients $d\eta_E/d\theta$ of the model with an exponential autocorrelation function markedly exceed the corresponding coefficients $d\eta_G/d\theta$ of the model with a Gaussian autocorrelation function at the scattering grazing angles $\tau = 5°–8°$ and

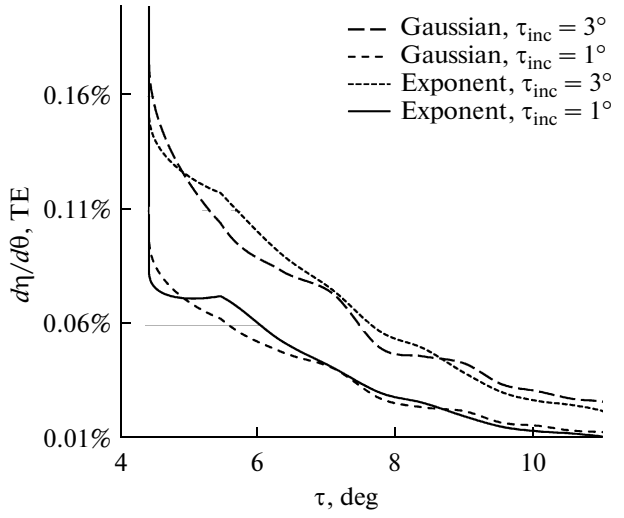

Fig. 1. Dependences between the intensity of the diffuse scattering at Au mirrors with different roughness statistics and the grazing angle of the scattered radiation at various grazing angles of incident radiation.

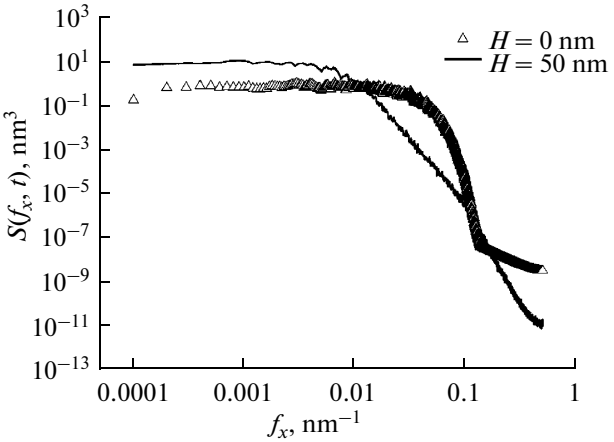

Fig. 2. PSDFs of a Si substrate roughness ($H = 0$) and an Al/Zr mirror 50 nm thick. The latter was constructed on the given substrate by means of simulation.

the two angles τ_{inc} indicated above. This is explained by the high "noisiness" of the boundaries with $D = 0.5$. The inflections of curves with $D = 0.5$ are not caused by physical actions and arise from insufficient discretization near the specular angle, where the scattering intensities of the two surface statistics under consideration are maximally different from each other. The detected discrepancies between the scattering intensities of mirrors with very similar surface topologies is evidence that, in practice, samples must be calculated with the help of an accurate roughness model. Therefore, the creation of high-quality mirrors and gratings requires the direct simulation of sample growth and the intensity of short-wavelength scattering thereof. Such a complex approach enables us to correctly determine changes in the small-scale roughness of interfaces due to source noise and growth processes; deformations observed during large-scale roughness (relief) growth, which substantially affects the grating efficiency; and the spectral intensity of scattering at multilayer mirrors and gratings with allowance for the complicated profiles of the formed boundaries.

Simulation of the Growth of Al/Zr Multilayer Mirrors

Let us investigate the influence of source noise on the surface roughness of an Al/Zr multilayer mirror. For simplicity, we consider the 2D isotropic problem in which boundary-profile height h depends only on spatial coordinate x and time t. In the study of multilayer-mirror growth, the equations describing the evolution of $h(x, t)$ must be numerically solved with allowance for the initial substrate boundary profile and the source noise. Afterward, with the help of the obtained data, function $S(f_x, t)$ should be determined from (12a) and quantities σ and ξ, from expressions (12b) and (12c). As an equation for the profile-shape evolution, let us choose (10) with strict allowance for local roughness. This is explained by the fact that, in the small-angle approximation reported in [8], (3) was demonstrated to describe variations in the surface roughness during Al/Zr multilayer-mirror growth under magnetron deposition. Therefore, (10) can provide the same accuracy of results.

The Al/Zr multilayer mirror was assumed to have the following parameters: $\Delta = 10.45$ nm and the ratio of the Zr-layer thickness to Δ is $\Gamma_{Zr} = 0.4$ [31]. The initial substrate roughness was accepted to be Gaussian (i.e., with a Gaussian autocorrelation function). In this case, calculations were carried out at different values of $\sigma(t = 0) = \sigma_0$ and $\xi(t = 0) = \xi_0$. The model mirror size was $L = 10$ μm, and the step was 1 nm. The source noise was specified by the fluctuation amplitude, the spatial length of the deposition inhomogeneity, and the noise inhomogeneity duration. The noise inhomogeneity length varied from 1 to 100 nm, and the inhomogeneity duration was chosen to be 1 s.

The calculated functions $S(f_x, t)$ averaged over seven implementations, which were determined at h_0 (substrate) and a grown multilayer-mirror height of $H =$ 50 nm, are depicted in Fig. 2. The profile evolution was calculated using the following parameters: $I_0 = 0.5$ nm/s, the noise amplitude is 0.2 nm/s, $\sigma_0 = 0.2$ nm, $\xi_0 = 10$ nm, $\nu_2(\text{Al}) = 1.0$ nm/s, $\nu_4(\text{Al}) = 125$ nm^3/s, $\nu_2(\text{Zr}) = 0.75$ nm/s, and $\nu_4(\text{Zr}) = 100$ nm^3/s.

From analysis of the dependences in Fig. 2, it follows that the autocorrelation function of the surface profile ceases to be Gaussian. In this case, the high-frequency component of roughness is smoothed (decreases) and its medium-frequency component makes a higher contribution. It is of interest that the PSDF ceases to correspond to the Gaussian statistics already at $H \sim 8$ nm. The PSDF of the mirror-boundary roughness exhibits analogous behavior, as is confirmed by AFM and TEM measurements, other

growth models, and X-ray scattering intensity measurements [8–11].

The time dependences of σ, which were determined at different values of σ_0, and ξ_0, are presented in Fig. 3a. The data were calculated using deposition and relaxation parameters similar to those of the example illustrated in Fig. 2. It was ascertained that averaging over four PSDFs is quite enough to attain convergence of the rms deviations of roughness.

As is apparent from Fig. 3a, the film profile evolution can be divided into two stages. At stage I, the dominant process is the smoothing of the initial roughness specified by the substrate. At stage II, the source noise makes the main contribution to changes in roughness. Let us analyze the behavior of the rms deviations of roughness during growth stage I when the mirror-boundary profile is smoothed due to surface diffusion defined by (3). For simplicity, the small-angle approximation is accepted to be valid (the character of reasoning remains unchanged if $\nabla h(x,t) \geq 1$. In the time Δt, the increment in profile height is $\Delta h(x, t+\Delta t) = h(x, t+\Delta t) - h(x, t)$. Therefore, (3) can be expressed as

$$\Delta h(x,t+\Delta t) = I_0 \Delta t + I(x,t)\Delta t - \nu_4 \nabla^4 h(x,t)\Delta t, \quad (14)$$

where $I(x, t)$ is the noise flux of atoms on the mirror surface. According to (14), upon short-duration deposition, the change in profile height due to the action of source noise in Δt, $\Delta h_n(x, t + \Delta t)$, (note that $\Delta h_n(x, t + \Delta t) = I(x, t)\Delta t$) is smaller than the profile change caused by smoothing of the initial relief, $\Delta h_i(x, t + \Delta t)$. Indeed, it can be assumed that $\Delta h_i(x, t + \Delta t) \approx \Delta^4 h(x, t = 0)\Delta t$ for short-duration depositions. Hence, $\Delta h_i(x, t + \Delta t) \gg \Delta h_n(x, t + \Delta t)$. In the case where t is small and σ is large, the following inequality holds true: $\Delta h_i(x, t + \Delta t) \gg \Delta h_n(x, t + \Delta t)$. Thus, changes related to the source noise increase during material deposition.

It follows from Fig. 3a that the larger the initial substrate roughness characterized by σ_0, the longer the influence of the initial relief on the growth process. Thus, the behavior of the mirror roughness alters within $t = 15$ and 0.1 s if $\sigma_0 = 0.3$ and 0.1 nm, respectively (see inset in Fig. 3a).

Let us consider how the initial correlation length of roughness affects changes in the film profile. The dependences of σ on t c σ_0, which were calculated at $\xi_0 = 0.1$ nm and different values of ξ_0, are depicted in Fig. 3b. As is seen in Fig. 3b, the roughness is approximately halved during the initial growth stage at $\xi_0 =$ 2 nm and the aforementioned value of σ_0. A decrease in σ is insignificant at $\xi_0 = 10$ nm. Such behavior is explained by the fact that relief asperities with the higher local curvature $K(x, t)$ of the surface (see (2) and (3)) are most strongly smoothed.

Let us estimate $K(x, t)$ if the growth duration is short. Under the assumption of the Gaussian statistics of roughness heights and a Gaussian autocorrelation function, the average slope angle γ_0 of the roughness

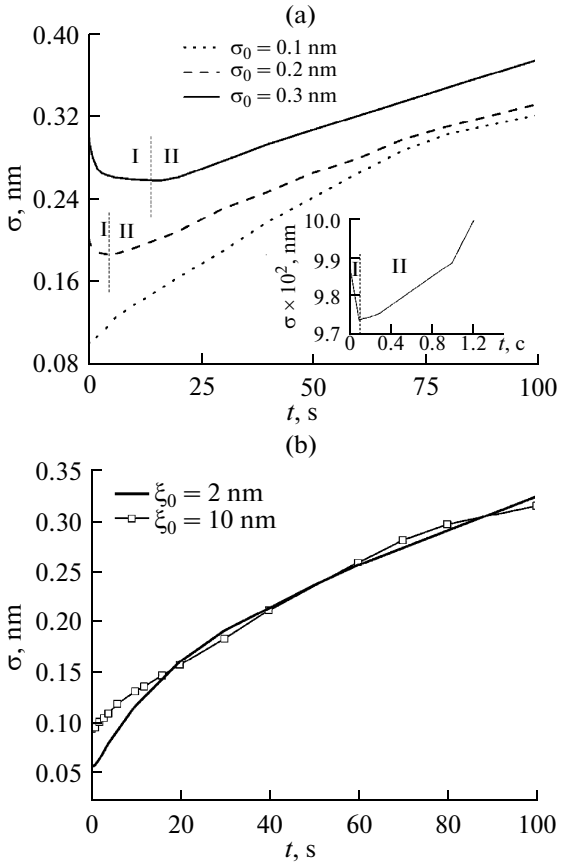

Fig. 3. Time dependences of the rms deviations of the Al/Zr mirror roughness: (a) the roughness correlation length is $\xi_0 = 10$ nm and the rms deviation σ_0 has different values and (b) $\sigma_0 = 0.1$ nm and ξ_0 has different values.

face is determined from the formula $\tan\gamma_0 = 2\sigma_0/\xi_0$. Since $\tan\gamma_0 = \nabla h$, the curvature of a single profile irregularity is defined as

$$K(x) = -\frac{\tan^2\gamma_0}{(1+\tan\gamma_0)^{3/2}}. \quad (15)$$

It follows from (15) that the larger γ_0, the larger the curvature of the profile irregularity. This implies that its irregularity is smoothed more substantially. Hence, a surface roughness with smaller ξ_0 is smoothed more strongly at identical values of σ_0.

Let us now estimate how the roughness correlation length varies with mirror size on the basis of fitting according to the K-correlation model defined by (12c). The dependences of length ξ on t, which were calculated at difference values of σ_0 and ξ_0, are presented in Fig. 4. As is clear from Fig. 4, mirrors with small roughnesses exhibit a more rapid increase in ξ at small thicknesses, i.e., if σ_0 and ξ_0 are small at insignificant roughness-face lengths. For large (deep and wide) roughnesses, an increase (spreading) in length ξ occurs more slowly during the initial growth stage. The correlation length of surface roughness determines the

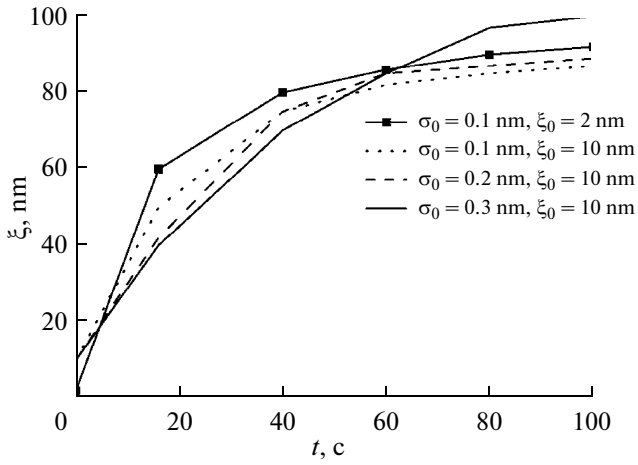

Fig. 4. Time dependences of the correlation length ξ of the Al/Zr mirror. Data were determined using the *K*-correlation model at different values of the rms deviation σ_0 of roughness and correlation length ξ_0 of the substrate.

lateral size of an asperity on the substrate and, consequently, the length that must be travelled by a diffusing atom located on the top to reach the asperity bottom. Larger roughnesses have the larger length mentioned above and, hence, are characterized by slower spreading at the beginning of growth. When roughnesses are sufficiently extended, deeper irregularities begin to spread more rapidly due to their larger height. It is seen from Fig. 4 that quantity ξ increases appreciably only up to a certain limit and takes a steady-state value at $H = 50$ nm.

Simulation of Triangular-Profile Multilayer Gratings

Triangular-profile diffraction gratings on Si substrates are manufactured using interference or electron-beam lithography and selective etching in which Si substrates cut at an angle of φ are treated in KOH solutions [21, 31–33]. The fabrication of large-scale gratings ($d \leqslant 200$ nm) of the short-wavelength range is promising. However, to implement the existing design potential, the fabrication process and technology must ensure the obtainment of almost ideally triangular grating grooves and coating preparation involving tens or hundreds of layers of atomic thickness with subatomically smooth boundaries. The decrease in η strongly depends on the profile smoothing effect, which manifests itself during multilayer-coating deposition and plays a critical role in short-period gratings. The achievement of shortest periods ($d \leqslant 200$ nm) is impossible if the influence of boundary parameters on the efficiency is not ascertained. Such an influence can be most easily determined by simulating growth boundaries and scattering intensities.

Triangular-profile grating growth was investigated as applied to magnetron and ion-beam deposition. The 2D problem typical of gratings with cylindrical groove geometry was considered. At the very beginning, the growth of a multilayer grating prepared on a Si substrate and having almost triangular groove profiles was simulated. The relaxation parameters of the growth model (see (2), (3), and (10)) were determined by comparing the measured upper boundaries of the grating profiles and their values obtained by simulation via the least squares method. Afterward, the profile boundaries were used as initial data to calculate the diffraction efficiency. The calculated efficiencies η(#) were compared with experimental data, and the model parameters, if necessary, were defined more precisely. Numerical experiments were conducted with the use of Mo/Si and Al/Zr gratings.

As in the preceding section, universal equation (10) was chosen to describe profile evolution because this relationship not only explicitly defines Al/Zr mirror growth but also correctly allows for the local surface roughness, i.e., enables us to simulate the large-scale grating relief growth.

Mo/Si Grating

Let us simulate a grating with $d = 136$ nm, $\varphi = 6°$, and 30 pairs of Mo/Si coating layers, for which a record-breaking efficiency of $\eta(-2) = 0.288$ was measured using a SR beam with $\lambda = 13.6$ nm at $\theta = 11°$ [32]. The period of the Mo/Si coating prepared by ion-beam deposition was 7 nm, and the quantity Γ_{Mo} was 0.45. The influence of the substrate and relaxation parameters (10) on changes in the profile of the growth boundaries was investigated with the help of averaged AFM measurements of profiles with 137 points located on the Si substrate and the upper boundary of the multilayer grating. To allow for appreciable transformation of the boundary profile during multilayer-coating deposition and achieve the desired accuracy of the solution to Eq. (10), the following parameters were employed in the growth simulation program: $I_0 = 0.6$ nm/s, $\nu_2(Mo) = 0.3$ nm/s, $\nu_4(Mo) = 0.5$ nm^3/s, $\nu_2(Si) = 0.3$ nm/s, and $\nu_4(Si) = 1.5$ nm^3/s. In this case, it was assumed that an atomic flux is vertically incident on the grating. The refractive indices of Mo and Si were taken in [34]. In the given example, the Debye–Waller amplitude factors [1, 7], which are similar to those of planar interfaces, were used to allow for random roughness and interdiffusion.

The calculated layer-boundary profiles (Fig. 5) indicate that the top and groove of the profile undergo some smoothing and the profile itself shifts to the left. The developed rigorous model used to calculate quantities η, which is combined with approximate determination of the influence of random boundary roughnesses, provides good coincidence between the efficiency of the principal diffraction order and the experiment performed with the help of a SR source in the examined wavelength range of 13.1–13.8 nm (Fig. 6). The efficiencies of other orders and incidence angles also coincided well, thereby confirming the

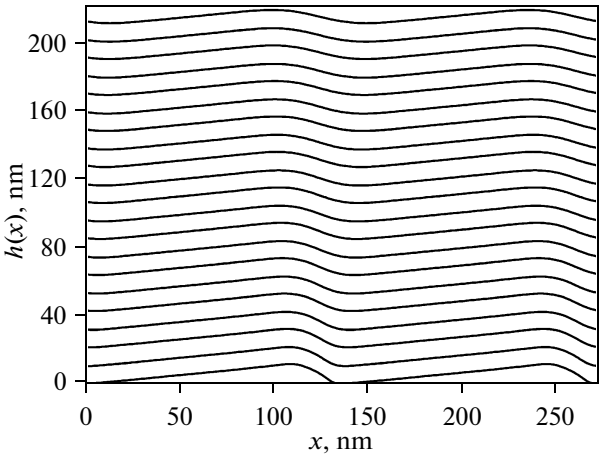

Fig. 5. Boundary profiles of a grating with a period of 136 nm, a blaze angle of 6°, and 30 pairs of Mo/Si coating layers whose period is 7 nm. Calculations were performed using the following parameters: $I_0 = 0.6$ nm/s, $\nu_2(\mathrm{Mo}) = 0.3$ nm/s, $\nu_4(\mathrm{Mo}) = 0.5$ nm^3/s, $\nu_2(\mathrm{Si}) = 0.3$ nm/s, and $\nu_4(\mathrm{Si}) = 1.5$ nm^3/s. For convenience, only a part of the boundary profiles is presented.

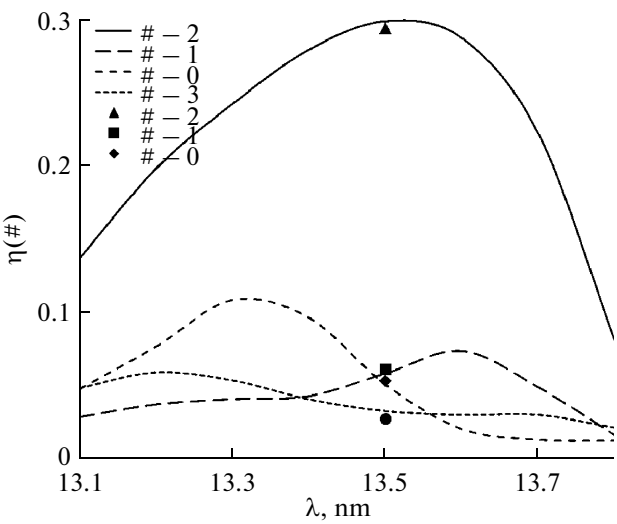

Fig. 6. Spectral efficiencies of the grating with parameters indicated in the caption of Fig. 5 at a radiation incidence angle of 11° near a wavelength of 13.5 nm: lines correspond to the model, and markers, to the experiment.

validity of the chosen model of multilayer-grating growth. The calculated and measured efficiencies can be more precisely correlated throughout the operating wavelength and incidence angle ranges by improving the model of the boundaries and strictly allowing for random roughness contributions.

For the calculations discussed above, good convergence of results is observed and $N = 200$ per boundary is required to simulate the quantity η of the grating having piecewise-linear boundaries with an error of no worse than 0.01%, which is estimated from the energy balance. When a low-end workstation with two Quad-Core Intel® Xeon® processors operating at a clock frequency of 2.66 GHz, a bus clock frequency of 1333 MHz, and 16 GB RAM is employed, one point is calculated in ~40 s.

Al/Zr Grating

It is most difficult to simulate an EUV grating with $d = 100$ nm, $\varphi = 6°$, and 20 pairs of Al/Zr coating layers deposited by magnetron sputtering. As was revealed by comparing the calculated and measured reflection coefficients of a multilayer mirror (witness), the parameters $\Delta = 10.43$ and $\Gamma_{\mathrm{Zr}} = 0.4$, which were included in the models of a multilayer Al/Zr grating coating, agree with the growth values and the average interface roughness is characterized by $\sigma \approx 0.9$ nm ($\sigma_0 \approx 0.4$ nm) [32, 33]. Moreover, the comparison data are evidence of ~90% TE polarization of the incident radiation (intensity).

To investigate how the substrate, the relaxation parameters in (10), and the deposition conditions affect variations in the profile of the growing boundaries, averaged AFM measurements of the profiles of the grating on a Si substrate and the upper boundary of a multilayer grating with ten periods and 1000 points were employed. The microscopy data of the AFM and TEM measurements were taken from [32, 33]. In this case, the feature of Al/Zr grating growth was associated with considerable transformation of the boundary profile: the profile height reduced to approximately one-third of the original value, intense smoothing was observed, and its top shifted to the right (Fig. 7). Such a profile change strongly contrasts with that inherent to Mo/Si grating growth, during which the profile var-

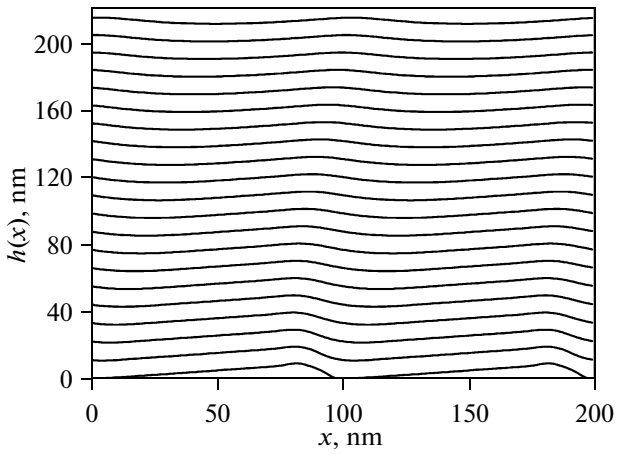

Fig. 7. Boundary profiles of a grating with a period of 100 nm, a blaze angle of 6°, and 20 pairs of Al/Zr coating layers whose period is 10.43 nm. Calculations were implemented using the following parameters: $I_0 = 0.6$ nm/s, $\nu_2(\mathrm{Zr}) = 0.2$ nm/s, $\nu_4(\mathrm{Zr}) = 5.0$ nm^3/s, $\nu_2(\mathrm{Al}) = 0.22$ nm/s, $\nu_4(\mathrm{Al}) = 7.0$ nm^3/s, and $\alpha = 78°$. For convenience, only a part of the boundary profiles is presented.

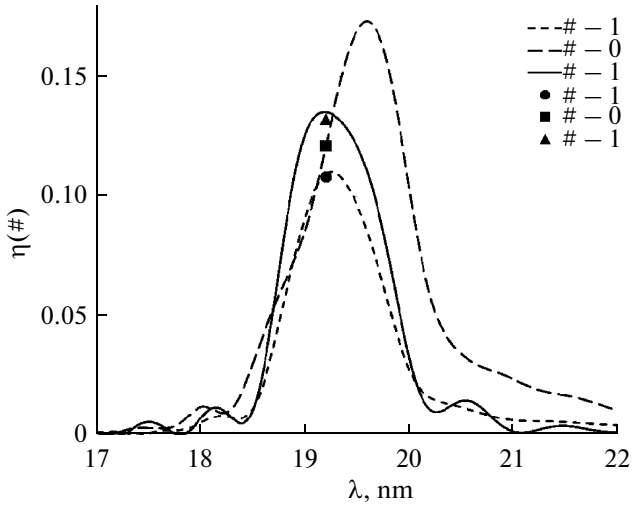

Fig. 8. Spectral efficiencies of the orders of the grating with the parameters indicated in the caption of Fig. 7 at a radiation incidence angle of 11°: lines correspond to the model, and markers, to the experiment.

ies much more weakly and shifts to the left (Fig. 5). This is explained by the oblique geometry of target-material deposition, which is used to prevent shadowing in the growth setup [21]. The simulation of Al/Zr grating growth demonstrates that the profile-top shift to the right is caused by the inhomogeneous fluxes of materials deposited onto the working and nonworking faces of a triangular profile due to the oblique impingement of deposited atoms on the substrate plane (at an angle differing from 90°). Significant smoothing of the boundary profile and the top shift were observed during growth simulation performed with the following parameters: $I_0 = 0.6$ nm/s, $\nu_2(\mathrm{Zr}) = 0.2$ nm/s, $\nu_4(\mathrm{Zr}) = 5.0$ nm^3/s,$\nu_2(\mathrm{Al}) = 0.22$ nm/s, $\nu_4(\mathrm{Al}) = 7.0$ nm^3/s, and $\alpha = 78°$. The strict approach of the growth model makes it possible to allow for the random roughness contribution, leading to a decrease in the efficiency of orders, as was determined by means of the PCGrate® program on the basis of the approach described in [6, 7].

The Al refractive indices were taken from [35], and Zr indices, from [34], because there were no data on Zr in [35]. As was ascertained in [25, 36, 37], the refractive indices of certain materials, which were determined with the help of the technique reported in [34], can be inaccurate in the examined wavelength range of 17–22 nm. The developed complex grating model, which enables us to estimate the influence of source inhomogeneity, the growth kinetics of deep asymmetric boundaries with large gradients, and the random roughness of boundaries with varying rms deviations and correlation lengths, provides very good agreement between the quantity η of the principal diffraction orders and the data measured at the SR source (Fig. 8). In the last case of measurements, $\theta = 36°$, $\lambda =$ 17.2 nm, and the difference between the measured efficiencies of the principal diffraction orders [31] and those calculated by simulation is less than 5%. For other values of θ and λ, coincidence also turned out to be good especially with allowance for the complexity of the used boundary model, the different phases of layers, their intermixing, and the lack of true values of the Zr refractive indices in the wavelength range under study. Calculations discussed above exhibit good convergence of the results, and, moreover, $N = 400$ is required to simulate the quantity η of a grating having randomly rough polygonal boundaries with an error of ~0.01% estimated from the energy balance. With the use of the aforementioned workstation, the time required to calculate one point is about 5 min.

CONCLUSIONS

This study demonstrates for the first time that the boundary growth of multilayer mirrors and gratings with a large height and jumps of the profile gradient can be correctly simulated by precisely allowing for the local curvature of the surface and the inhomogeneity of material deposition on the substrate. Owing to efficient algorithms and the potential of the developed vector electromagnetic PCGrate code, a standard PC can be employed to examine diffraction gratings and mirrors. The investigations are carried out with the help of data obtained by the simulation of boundary-profile growth and provide theoretical results making it possible to predict the intensities of X-ray and extreme UV scattering ay multilayer gratings and mirrors with an accuracy equivalent to that of measurements based on synchrotron radiation. The proposed complex numerical simulation enables us to abruptly decrease the costs of technological processes and measurements performed during the manufacture of multilayer diffraction gratings and mirrors with the required boundary surface structure to achieve values of η close to the theoretical limit [38, 39].

The boundary integral approach is extended to analysis of the intensity of short-wavelength scattering by multilayer diffraction gratings and mirrors and can be efficiently applied to research into various gratings intended for operation in other spectral ranges, photonic crystals, Fresnel-zone plates, and rough mirrors. In turn, the multilayer film growth model can be employed to study growth processes in semiconductor structures, namely, superlattices, buffer layers, low-dimensional nanostructures, etc. The performed investigations are useful from the viewpoint of designing high-resolution instruments for X-ray spectroscopy of the Sun and other nonterrestrial objects, studies of plasma physics, X-ray lithography, X-ray correlation spectroscopy, resonant inelastic X-ray spectroscopy, and other fields of science and technology.

ACKNOWLEDGMENTS

The authors are grateful to D.L. Voronov, Yu.V. Trushin, and V.V. Yashchuk for useful discussions and the provision of information.

REFERENCES

1 1. U. Pietsch, V. Holy, and T. Baumbach, *High-Resolution X-Ray Scattering: From Thin Films to Lateral Nanostructures* (Springer, Heidelberg, 2004).
2. L. I. Goray, Proc. SPIE **8083**, 80830 (2011).
3. *Light Scattering and Nanoscale Surface Roughness,* Ed. by A. A. Maradudin (Springer, New York, 2007).
4. L. I. Goray, Proc. SPIE **7390**, 73900V (2009).
5. L. I. Goray, J. F. Seely, and S. Yu. Sadov, J. Appl. Phys. **100**, 094901 (2006).
6. L. I. Goray, J. Appl. Phys. **108**, 033516 (2010).
7. L. I. Goray, Waves Random Media **20**, 569 (2010).
8. D. L. Voronov, P. Gawlitza, R. Cambie, E. M. Gullikson, F. Salmassi, T. Warwick, V. V. Yashchuk, and H. A. Padmore, Proc. SPIE **8139**, 81390B (2011).
9. L. Peverini, E. Ziegler, and I. Kozhevnikov, Appl. Phys. Lett. **91**, 053121 (2007).
10. D. G. Stearns, D. P. Gaines, D. W. Sweeney, and E. M. Gullikson, J. Appl. Phys. **84**, 1003 (1998).
11. L. Goray and J. Seely, Appl. Opt. **41**, 1434 (2002).
12. M. Pellicione and T.-M. Lu, *Evolution of Thin Film Morphology. Modelling and Simulations* (Springer, Berlin, 2008).
13. M. N. Lubov, D. V. Kulikov, and Yu. V. Trushin, Phys. Status Solidi C **7**, 378 (2010).
14. V. S. Kharlamov, Y. V. Trushin, E. E. Zhurkin, M. N. Lubov, and J. Pezoldt, Tech. Phys. **1**, 1490 (2008).
15. J. M. Haile, *Molecular Dynamics Simulation* (Wiley, New York, 1997).
16. F. Jensen, *Introduction to Computational Chemistry* (Wiley, New York, 2006).
17. M. Kotrla, Comput. Phys. Commun. **97**, 82 (1996).
18. W. W. Mullins, J. Appl. Phys. **28**, 333 (1957).
19. J. W. Gibbs, The Sci. Papers, 55 (1906).
20. M. Kardar, G. Parisi, and Y.-Ch. Zhang, Phys. Rev. Lett. **56**, 889 (1986).
21. D. L. Voronov, M. Ahn, E. H. Andesrson, R. Cambie, Ch.-H. Chang, L. I. Goray, E. M. Gullikson, R. K. Heilmann, F. Salmassi, M. L. Schattenburg, T. Warwick, V. V. Yashchuk, and H. A. Padmore, Proc. SPIE **7802**, 780207 (2010).
22. J. C. Stover, *Optical Scattering* (SPIE Press, Bellingham, Washington, DC, 1995).
23. L. I. Goray and G. Schmidt, J. Opt. Soc. Am. A **27**, 585 (2010).
24. L. I. Goray and G. Schmidt, Phys. Rev. E **85**, 036701 (2012).
25. PCGrate. http://www.pcgrate.com. Cited March 1, 2013.
26. A. Rathsfeld, G. Schmidt, and B. H. Kleemann, Commun. Comput. Phys. **1**, 984 (2006).
27. E. Popov, B. Bozhkov, D. Maystre, and J. Hoose, Appl. Opt. **38**, 47 (1999).
28. *Electromagnetic Theory of Gratings*, Ed. by R. Petit (Springer, Berlin, 1980).
29. L. I. Goray, Nucl. Instrum. Methods Phys. Res. A **536**, 211 (2005).
30. L. I. Goray and S. Yu. Sadov, *Diffractive Optics and Micro-Optics*, OSA Trends in Optics and Photonics Series, Vol. 75 (DC, Washington, DC, 2002), p. 365.
31. D. L. Voronov, E. H. Anderson, R. Cambie, S. Cabrini, S. D. Dhuey, L. I. Goray, E. M. Gullikson, F. Salmassi, T. Warwick, V. V. Yashchuk, and H. A. Padmore, Opt. Express **19**, 6320 (2011).
32. D. L. Voronov, P. Gawlitza, R. Cambie, S. Dhuey, E. M. Gullikson, T. Warwick, S. Braun, V. V. Yashchuk, and H. A. Padmore, J. Appl. Phys. **111**, 093521 (2012).
33. D. L. Voronov, E. H. Anderson, E. M. Gullikson, F. Salmassi, T. Warwick, V. V. Yashchuk, and H. A. Padmore, Opt. Lett. **37**, 1628 (2012).
34. Center of X-Ray Optics. http://henke.lbl.gov/optical_constants/. Cited March 1, 2013.
35. *Handbook of Optical Constant of Solids*, Ed. by E. D. Palik (Academic, New York, 1985).
36. J. Seely, L. Goray, D. Windt, B. Kjornrattanawanich, Y. Uspenskii, and A. Vinogradov, Proc. SPIE **5538**, 43 (2006).
37. K. Le Guen, M.-H. Hu, J.-M. André, P. Jonnard, S. K. Zhou, H. Ch. Li, T. Zhu, Z. S. Wang, N. Mahne, A. Giglia, and S. Nannarone, Appl. Phys. A: Mater. Sci. Process. **102**, 69 (2011).
38. L. I. Goray, J. Surf. Invest.: X-Ray, Synchrotron Neutron Tech. **2**, 796 (2008).
39. L. I. Goray, J. Surf. Invest.: X-Ray, Synchrotron Neutron Tech. **1**, 362 (2007).

Translated by S. Rodikov

SPELL: 1. ok